Source details

Asia-Pacific Journal of Science and Technology

Scopus coverage years: from 2017 to Present

Publisher: Khon Kaen University,Research and Technology Transfer Affairs Division

E-ISSN: 2539-6293

Subject area: Agricultural and Biological Sciences: General Agricultural and Biological Sciences | Engineering: General Engineering

Source type: Journal

CiteScore 2022
1.0

SJR 2022
0.151

SNIP 2022
0.260

View all documents > | Set document alert | Save to source list | Source Homepage

CiteScore | CiteScore rank & trend | Scopus content coverage

Improved CiteScore methodology

CiteScore 2022 counts the citations received in 2019-2022 to articles, reviews, conference papers, book chapters and data papers published in 2019-2022, and divides this by the number of publications published in 2019-2022. Learn more >

CiteScore 2022

1.0 = 234 Citations 2019 - 2022 / 245 Documents 2019 - 2022

Calculated on 05 May, 2023

CiteScoreTracker 2023

0.8 = 229 Citations to date / 275 Documents to date

Last updated on 05 September, 2023 • Updated monthly

CiteScore rank 2022

Category	Rank	Percentile
Agricultural and Biological Sciences └ General Agricultural and Biological Sciences	#153/213	28th
Engineering └ General	#234/302	22nd

View CiteScore methodology > | CiteScore FAQ > | Add CiteScore to your site

ISSN 2539-6293

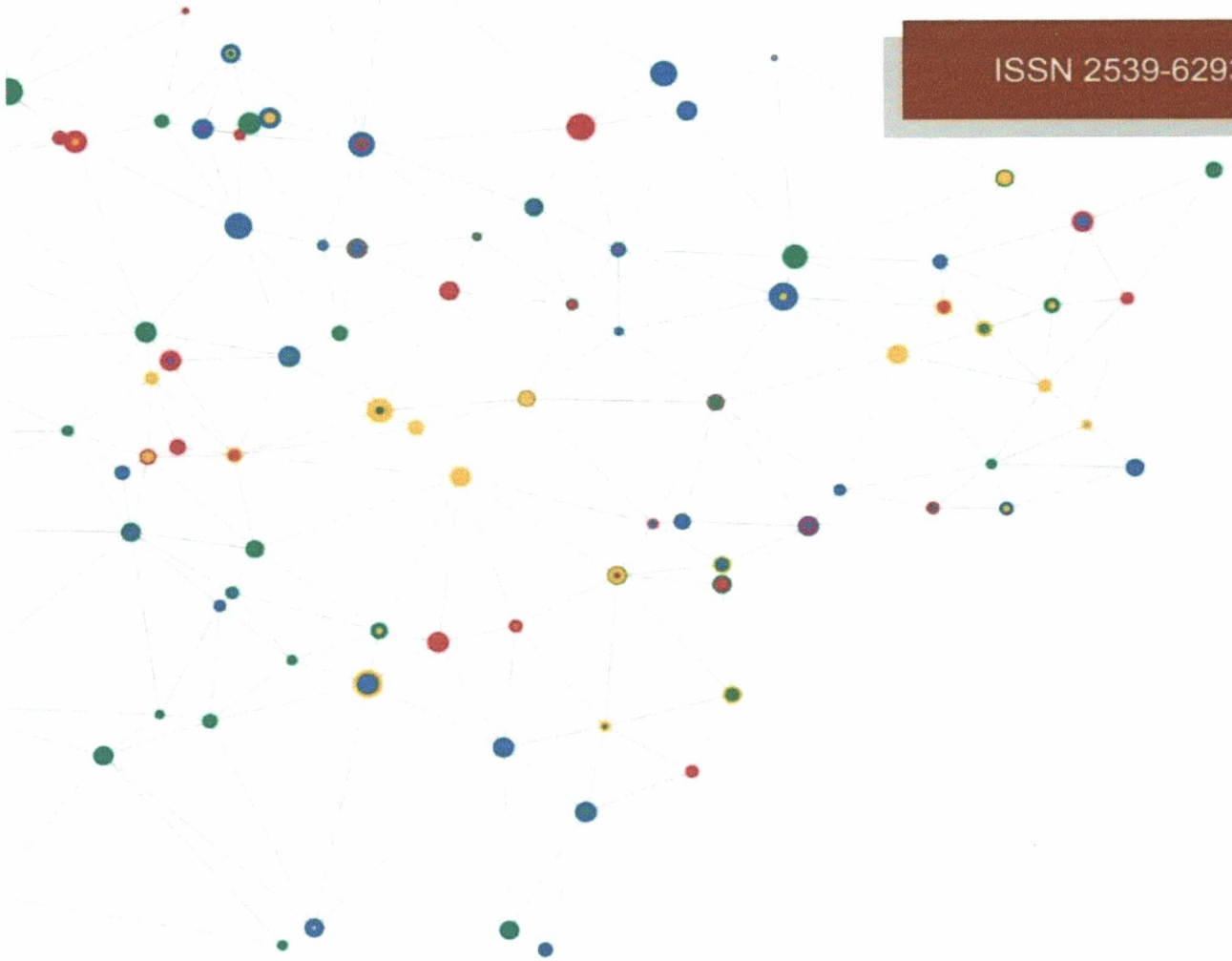

APST

Asia-Pacific Journal of Science and Technology

APST
Asia-Pacific Journal of
Science and Technology

(https://so01.tci-thaijo.org/index.php/APST/issue/view/17434)

Published: 2023-04-24

Research Articles

Differential activity of vermicompost and plant growth regulators (GA3 and IAA) on yield and growth parameters of Zingiber officinale rosc (https://so01.tci-thaijo.org/index.php/APST/article/view/266852)

Vasavirama Karri, Nagasi A. Nidumolu, Nirmala Nalluri

APST-28-02-06 (11 pages)

PDF (https://so01.tci-thaijo.org/index.php/APST/article/view/266852/173317)

Purification and characterization of laccase from Ganoderma sp. 03 (https://so01.tci-thaijo.org/index.php/APST/article/view/250626)

Rakrudee Sarnthima, Watchara Kanchanarach, Saranyu Khammuang

APST-28-02-07 (8 pages)

PDF (https://so01.tci-thaijo.org/index.php/APST/article/view/250626/173632)

Repair welding of 6082-T6 aluminum alloy through MIG and TIG processes (https://so01.tci-thaijo.org/index.php/APST/article/view/252876)

Prapas Muangjunburee, Thongchai Khrueaphue

APST-28-02-08 (9 pages)

PDF (https://so01.tci-thaijo.org/index.php/APST/article/view/252876/173492)

Safety effectiveness of an upgraded midblock pedestrian crossing on an urban arterial road (https://so01.tci-thaijo.org/index.php/APST/article/view/254404)

Pongsatorn Pechteep, Paramet Luathep, Nopadon Kronprasert, Sittha Jaensirisak

APST-28-02-09 (12 pages)

PDF (https://so01.tci-thaijo.org/index.php/APST/article/view/254404/173320)

Characterization of glycoconjugates in giant freshwater prawn embryos by lectin histochemistry (https://so01.tci-thaijo.org/index.php/APST/article/view/252623)

Noppakun Pakdeenarong

APST-28-02-10 (7 pages)

PDF (https://so01.tci-thaijo.org/index.php/APST/article/view/252623/173321)

A deep learning model for air leak detection from a pipe fitting using an accelerometer (https://so01.tci-thaijo.org/index.php/APST/article/view/253464)

Thanakrit Kraising, Winai Wongthai, Thanathorn Phoka, Aimaschana Niruntasukrat, Nuttanat Ruttanapahat

APST-28-02-11 (14 pages)

PDF (https://so01.tci-thaijo.org/index.php/APST/article/view/253464/173322)

Different fit factors for the N95 respirator during endotracheal intubation: Comparing video laryngoscopy and direct laryngoscopy (https://so01.tci-thaijo.org/index.php/APST/article/view/256223)

Khontorn Jankusol, Naesinee Chaiear, Thapanawong Mitsungnern

APST-28-02-12 (10 pages)

PDF (https://so01.tci-thaijo.org/index.php/APST/article/view/256223/173337)

Characterization of a recombinant arylsulfatase enzyme from glucosinolate-metabolizing human gut bacterium Escherichia coli VL8 (https://so01.tci-thaijo.org/index.php/APST/article/view/252493)

Vijitra Luang-In, John T. Rossiter, Abdulhadi A. Albaser

APST-28-02-13 (9 pages)

PDF (https://so01.tci-thaijo.org/index.php/APST/article/view/252493/173374)

The remote monitoring of aflatoxin levels in grain corn relative to temperature and humidity (https://so01.tci-thaijo.org/index.php/APST/article/view/250336)

Aina Shahrul, Huraiyah Shariruzi, Ilia N. Rirezal, Anas M. Mustafah, Nik I. P. Samsudin, Jinap Selamat, Nurulhuda Khairudin, Maimunah Sanny

APST-28-02-14 (10 pages)

PDF (https://so01.tci-thaijo.org/index.php/APST/article/view/250336/173339)

Adsorption of PM2.5 emissions from laser printer by paper waste aerogel (https://so01.tci-thaijo.org/index.php/APST/article/view/266881)
Nanthana Chanthorn, Thanathorn Petchrat, Titiwud Pongtanapaisan, Sirikarn Thongmai, Thanakrit Neamhom
APST-28-02-15 (10 pages)
PDF (https://so01.tci-thaijo.org/index.php/APST/article/view/266881/173340)

Recombinase polymerase amplification for human male determination from semen (https://so01.tci-thaijo.org/index.php/APST/article/view/264434)
Anupong Sukjai, Monthira Monthatong
APST-28-02-16 (8 pages)
PDF (https://so01.tci-thaijo.org/index.php/APST/article/view/264434/173342)

Make a Submission (https://so01.tci-thaijo.org/index.php/APST/about/submissions)

Home ThaiJo

THAIJO (https://www.tci-thaijo.org/)

Manual

For Author (https://drive.google.com/drive/folders/16k9oDDz1lRHtD9bFD2oRcRSiitqctb0s?usp=sharing)

For Reviewer (https://drive.google.com/open?id=1Zu9fZFXCBNP_MvBGRPlDaUURyznknWAu)

Instructions

Instructions for authors (https://www.tci-thaijo.org/index.php/APST/Instructions)

Information

For Readers (https://so01.tci-thaijo.org/index.php/APST/information/readers)

For Authors (https://so01.tci-thaijo.org/index.php/APST/information/authors)

For Librarians (https://so01.tci-thaijo.org/index.php/APST/information/librarians)

Indexed In

Scopus (https://www.scopus.com/sourceid/21100871804)

1.0 CiteScore 2022
28th percentile
Powered by Scopus
(https://www.scopus.com/sourceid/21100871804)

TCI ศูนย์ดัชนีการอ้างอิงวารสารไทย Thai-Journal Citation Index Centre
(https://tci-thailand.org/list%20journal.php)

ASEAN CITATION INDEX
(https://asean-cites.org/list_of_journal.html)

DOAJ DIRECTORY OF OPEN ACCESS JOURNALS
(https://doaj.org/toc/2539-6293?source=%7B%22query%22%3A%7B%22filtered%22%3A%7B%22filter%22%3A%7B%22bool%22%3A%7B%22must%22%3A%5B%7B%26293%22%5D%7D%7D%2C%7B%22term%22%3A%7B%22_type%22%3A%22article%22%7D%7D%5D%7D%7D%2C%22query%22%3A%

Asia-Pacific Journal of Science and Technology,
The Research Administration Division
Office of the President 2, Building 2
Khon Kaen University, Khon Kaen, 40002
Tel. +66 (0) 4320 3178
E-mail: apst.kku@gmail.com

Asia-Pacific Journal of Science and Technology: Volume: 28. Issue: 02. Article ID.: APST-28-02-08. Research Article

APST **Asia-Pacific Journal of Science and Technology**

https://www.tci-thaijo.org/index.php/APST/index

Published by the Research and Graduate Studies,
Khon Kaen University, Thailand

Repair welding of 6082-T6 aluminum alloy through MIG and TIG processes

Prapas Muangjunburee[1,2] and Thongchai Khrueaphue[3,*]

[1]Department of Mining and Materials Engineering, Faculty of Engineering Prince of Songkhla University, Songkhla, Thailand
[2]Center of Excellence in Metal and Materials Engineering (CEMME), Faculty of Engineering Prince of Songkhla University, Songkhla, Thailand
[3]Program in Production Technology, Faculty of Agricultural and Industrial Technology, Phetchabun Rajabhat University, Petchabun, Thailand
*Corresponding author: Thongchai.k@PCRU.ac.th

Received 7 December 2021
Revised 8 April 2022
Accepted 21 April 2022

Abstract

In this study, the 6082-T6 aluminum alloy was repaired by Metal Inert Gas (MIG) and Tungsten Inert Gas (TIG) welding using the filler ER 4043. The influences of thermal heat cycles on the microstructure and mechanical properties of weldments produced by different welding processes were assessed based on macrostructure, microstructure, tensile and micro-hardness tests. The experimental results revealed that the tensile strengths of the TIG and MIG welded joints were 199.6 MPa and 172.2 MPa, respectively, which were reduced after repair welding to 178.9 MPa and 168.1 MPa, respectively. The tensile strength of TIG welded joints were lower than those of MIG welded joints due to the lower hardness in the heat-affected zones (HAZs) due to high TIG heat input. The tensile strength was decreased after repair welding irrespective of the welding processes due to the double over-ageing effect in the over-ageing zones. These results suggest that MIG welding process should be preferred for the repair welding of 6082-T6 aluminum alloy.

Keywords: 6082-T6 aluminum alloy, Repair welding, Mechanical properties, MIG welded joints, TIG welded joints

1. Introduction

Aluminum alloys are extensively utilized in transportation industries such as rolling stocks, vehicle structures, and ship structures due to their attractive combination of physical and chemical properties (lightweight, high strength, good corrosion resistance, good weldability, and formability) [1,2]. Among them, 6082-T6 aluminum alloy is a heat-treatable alloy that can be strengthened to provide moderate mechanical strength [3,4]. In the assembling of aluminum alloy structural parts, the joining of such parts is inevitably performed by different welding processes in the industrial production. Metal Inert Gas Welding (MIG) and Tungsten Inert Gas (TIG) welding are the widely used fusion welding processes for joining of such structural components into a different dimensional assembly owing to easy operation and high productivity [5,6].

The welding of the aluminum alloys, especially in the fusion welding, generates a variety of problems such as porosity formation, liquation cracks, lack of fusion, low production efficiency, weld distortion and joint softening due to its strong thermal conductivity, large thermal expansion coefficient, the formation tendency of refractory oxide, high solubility of hydrogen in the liquid aluminum, low stiffness, and the divergent heat source. It is generally accepted that TIG welding process can provide better weld quality than MIG [7]. However, MIG welding process can be possible to function semi-automatic operating mode with its comparatively easier applicability, better economy with the availability of high welding speed and suitability to operate long continuous welds on heavy gauge objects, making it as the dominant welding technology in industrial sector [5,6]. In the solid-state welding namely, Friction Stir Welding (FWS) which is not required liquid phase cooling during

welding, the welding defects such as porosity, solution redistribution, distortion and liquation cracking can be avoided and the joints with better mechanical strength can be produced [8,9]. However, this welding method has some limitation such as the selection of appropriate shape and specific material of a tool must be required and the plates to be joined must be tightly fastened, limiting the flexibility of the process to some extent [10,11]. In the fusion welding of 6082-T6 aluminum alloys, there are three main challenges needed to be controlled by the welders, which detrimentally deteriorate the mechanical performance of the joints: porosity formation [12], liquation cracking [13] and softening effect in the heat-affected zone (HAZ) [14]. Porosity introduced in the weld zone (WZ) is primarily related to the high solubility of hydrogen in the molten state of aluminum during welding. Liquation cracking occurs due to the combined effect of thermal stress and solidification shrinkage of the liquid aluminum generated during welding. Generally, these types of defects that induce large residual stresses and decrease the strength of the welded joints can be eliminated or reduced by optimizing the welding conditions and parameters. However, the mechanical weakness in the HAZ through welding thermal cycles is unavoidable in aluminum welding because the induced welding temperature above ~0.7 Tm can be over-aged the HAZ within in a few seconds [15]. Metallurgical transformations and/or softening due to over-ageing of strengthening precipitates makes the HAZ of 6082-T6 aluminum alloys weakened and consequently, the reduction of mechanical strength of welded joints, especially in the repair joints, is occurred.

The repair welding is performed whenever it is necessary for not only maintenance of welded structures to extend the service life but also fixing of poor welded structures with one or more welding defects, such as pores and cracks [16,17]. The repair joints will suffer twice as much the over-ageing effect in the HAZ because of additional thermal cycles of repairing and as a result, the repair joints may be further strength reduction. Few studies are available in the literature about the mechanical properties of repair welding of aluminum alloys. The groove defect in aluminum alloy (AA) 2219 welds made by FSW was repaired by Liu et al [18] It was reported that the tensile strength of repair joints was weakened due to the formation of fine cavity defects and aggregation of brittle Al_2Cu phases. Katsas et al [17] studied microstructural changes in fusion zone after repair welding in AA 5xxx using ER 5183 filler by MIG welding and reported that grain coarsening and porosity in the fusion zone weakened the mechanical properties of repair joints. Shankar et al [16] investigated fatigue crack behavior in repair welding of AA 5083 welds by MIG welding and found out that the residual fatigue life of the welded joints was decreased due to the larger size and greater amount of defects introduced after repair welding. Thus, during repair welding, microstructural transformations and defects may further be introduced in the weld joints due to the additional thermal cycles during welding, and thereafter lead to a weakened joint compared to the original sound weld [19,20]. Therefore, special attention should be paid on the effect of welding thermal cycles of AA 6082-T6 repair welding and their related mechanical properties. The repair weldments can provide the required quality or not is still unknow while the reliability and safety are priority in transportation services.

Extensive research in the conventional TIG welding process has been recently available in the literature [23-25]. Baskutis et al [21] explored the tensile strength of the TIG-welded AA 6082-T6 joints by varying the groove angles of the plates and welding currents. Wan et al [22] optimized the tensile strength of the TIG-welded joints of aluminum alloy by controlling the weld geometry such as penetration depth, weld width and weld reinforcement. Shanavas et al [23] investigated the influence of TIG welding currents and gas flow rate on the tensile strength of AA 5052 H32 plates and compared it with the welded joint produced by FWS. Chaurasia et al [24] studied the residual stress and mechanical properties of the welded joints produced by TIG and FWS. Sirohi et al [25] prepared the dissimilar welded joint of modified 9Cr-1Mo and SS 304 using TIG process and studied the effect of post-weld heat treatment on metallurgical and mechanical properties. Pandey et al [26] studied the softening mechanism of TIG-welded P91 steel by performing two different types of heat treatments including the post-weld direct tempering (PWDT) and re-austenitizing based tempering (PWNT). Pandey et al [27] also examined the relation of microstructural evolution and mechanical behavior of TIG-welded P92 steel subjected to PWDT. From the literature, no study has researched the effect of repeated thermal cycles on the microstructure and mechanical properties of repair welding of AA 6082-T6 weldments. Moreover, there is rarely reported that how the two different fusion welding processes contributed on their properties.

This study investigated the microstructural and mechanical properties of repair weldments of AA 6082-T6 by MIG and TIG welding processes using ER 4043 filler to explore how the two different welding processes influence on the mechanical characteristics of repair welds of an aluminum alloy, by examining the physical appearance and weld profile, microstructure, and hardness, tensile properties.

2. Materials and methods

In this study, AA 6082-T6 plate with a thickness of 6 mm was employed as the base material, and Erbium (ER) 4043 with 1.2 mm diameter as the consumable filler. The chemical compositions and mechanical properties of the base material and the filler are shown in (Table 1). Firstly, AA 6082-T6 plates were cut into the dimensions of 300 x150 mm. Then, the plates were welded in a butt joint position with a groove angle of 60° having a root opening of 1 mm, as shown in (Figure 1). Before welding, the aluminum plates and filler were carefully cleaned

using stainless steel brush wire followed by acetone cleaning, to make free from surface impurities such as oxides, grease, oil, and dust.

Table 1 Chemical compositions and mechanical properties of AA 6082-T6 and ER 4043 filler [28].

AA 6082-T6	Chemical composition	Elements (%)								
		Si	Fe	Cu	Mn	Mg	Cr	Zn	Ti	Al
		0.7-1.3	0.50	0.10	0.4-1.0	0.6-1.2	0.25	0.20	0.10	Bal.
	Mechanical properties	Tensile strength (MPa)		Yield strength (MPa)		Elongation (%)		Hardness high voltage [HV]		
		310		260		6		110		
ER 4043	Chemical composition	Elements (%)								
		Si	Fe	Cu	Mn	Mg	Cr	Zn	Ti	Al
		4.5-6.0	0.15	0.03	0.007	0.003	0.001	0.004	0.01	Bal.
	Mechanical properties	Tensile strength (MPa)		Yield strength (MPa)		Elongation (%)		Hardness [HV]		
		165		130		1.2		60		

MIG welded joints were prepared using MIG direct current electrode positive (DCEP) with a constant welding DC current of 135 A, an applied welding arc voltage of 20 V and a travel speed of 55 cm/min. Pure argon (>99.999% purity, Grade 5.0) was used as the shielding gas with a flow rate of 25 L/min. TIG welded joints were generated using alternating current polarity, and the welding AC current and arc voltage were set to 160 A and 15 V with a travel speed of 20 cm/min. The shielding gas (pure argon) was supplied at a flow rate of 15 L/min. For the as-welds (AWs), the first (1) and second passes (2) were welded on the beveled side, then back-gouged by grinding and welded for the third pass (3). After that, the repair welds (RWs) were made by re-welding after removing the passes of the AW by grinding. Joint details and sequence of processing the passes are illustrated in (Figure 1, 2). The AW and RW made by MIG welding process were denoted as MIG AW and MIG repair weld (RW), and those made by TIG welding process were denoted as TIG AW and TIG RW, respectively.

All welded joints were cross-sectioned, ground with SiC paper up to 2,500 grits, and polished using 1 μ alumina solution and etched with Keller's reagent in accordance with standard metallographic technique. The physical appearance of weld beads was firstly observed by visual inspection to make sure that the applied welding parameters produced the good joints. The weld profiles were observed under an optical microscope (Olympus SZ2-ET). The grain size was evaluated by the lineal intercept method [29]. An optical microscope (Olympus Scope.A1) was used to distinguish the microstructures of the welded joints. Tensile strength was evaluated by tensile tester (Hounsfield model H100KS universal machine) according to the standard AWS D1.2 [30]. Hardness was measured on Zwick/Roell ZHU hardness tester at every 1 mm interval under a constant load of 100 gram force (GF) along the transverse section of welding parts through weld metals (WMs), HAZ and the base metal (BM).

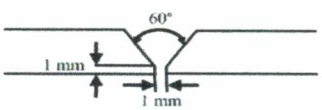

Figure 1 Welded joint geometry.

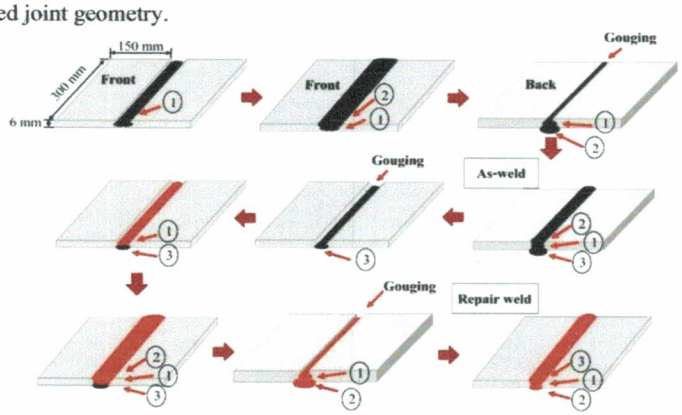

Figure 2 Sequence of the weld passes for AW and RW.

3. Results and discussion

3.1 Physical appearance

The physical appearance of weldments produced by MIG and TIG welding are shown in (Figure 3). It could be observed that both the MIG and TIG welded joints showed the good weld appearance before and after repair welding. In addition, the smooth and homogeneous surfaces of the weldments were observed in the MIG welded passes while the weld bead patterns were more distinct in the TIG welded passes. All welded joints were free from defects such as crack, undercut, slag inclusion, lack of penetration and lack of fusion.

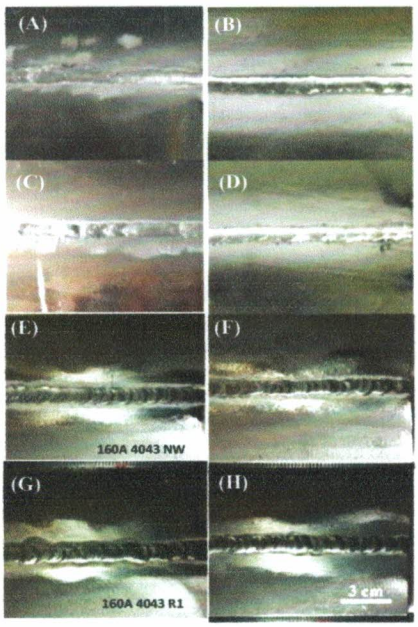

Figure 3 Physical appearance of weldments made by MIG and TIG welding: (A) front side and (B) back side of MIG AW, (C) front side and (D) back side of MIG RW, (E) front side and (F) back side of TIG AW, and (G) front side and (H) back side of TIG RW.

Figure 4 shows the cross-sections of the MIG and TIG welded joints before and after repair welding. (It could be observed that) all welded joints exhibited good penetration. However, some defects were also formed in TIG welded joints. The good weld reinforcement was found on MIG welded samples while the uneven and excessive reinforcement was observed on the TIG welded samples. In addition, concave structures of the weld passes were also appeared in the TIG welded samples. This is related to the high applied TIG welding current and low welding voltage.

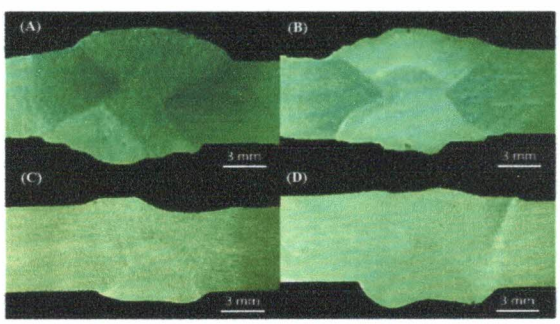

Figure 4 Cross-sectional image of weldments; (A) MIG AW, (B) MIG RW, (C) TIG AW and (D) TIG RW.

3.2 Microstructures of the welded joints

Microstructures of BM, HAZs and WMs of the MIG and TIG welded joints are shown in (Figure 5, 6), respectively. BM microstructure (Figure 5A) indicated the distribution of second phase particles in the rolling direction in the matrix aluminum α solid solution. The HAZ and WM microstructures of the MIG as- AW and RW are illustrated in (Figures 5 B, 5C and 5D, 5E) whereas those of TIG AW and RW are illustrated in (Figures 6A, 6B and 6C, 6D). In all joints, it was evident that the directional solidification of the weld by the variation of grain structures from edge to weld center during welding. The microstructure evolution at the fusion zone (FZ) could be characterized by epitaxial nucleation and growth. The elongated grains appeared at the edges of the weld where the solidification process started first and equiaxed grains at the WM where the solidification ended. As expected, the grain sizes and grain structures of WM remained almost unchanged after repair welding in both MIG and TIG welds. The weld passes on the front side of the RW were repaired after removing mechanically that of AW, resulting in an identical microstructure in that zone. However, in the MIG welded joints, the grainy dendrite structures were formed in the WM whereas a fraction of non-equiaxed dendrite structures was included in the WM of the TIG welded joints. On the other hand, in the partially melting zones (PMZs), wider grains appeared in the TIG welded joints. This is directly related to its heat input experienced by the base metal, which can be expressed by the following Equation 1 [31,32]:

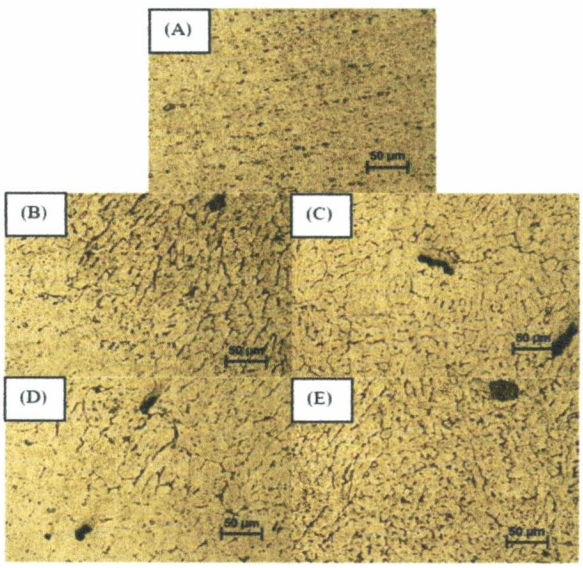

Figure 5 Microstructures of the MIG welded joints before and after repair welding: (A) BM, (B) HAZ AW, (C) WM AW, (D) HAZ RW and (E) WM RW.

$$Q = VI/(1{,}000\ S)\ \eta \quad (1)$$

where, Q is heating input (kJ/mm), η is the thermal efficiency (0.6), S is welding speed (mm/min) and V and I are the applied arc voltage (V) and welding current (A), respectively.

The higher heat input generated in TIG welding made the grains in PMZs wider than those for MIG welding. In addition, the change in HAZ zone microstructures was observed after repair welding as shown in (Figure 5B, 5D), and (Figure 6A, 6C). The HAZ can be divided into two sub-zones: the one near the fusion line is specified as PMZ and the other one far from the fusion line as an over-ageing zone (OZ). The enlarged grains could be visible at PMZ near the fusion line after repair welding irrespective of welding processes. This could be attributed to double welding thermal cycles in the HAZ of the RWs compared with the AWs. In addition, in the OZ, the over-ageing of strengthening precipitates was microstructurally observed in the TIG welded joints before and after repair welding.

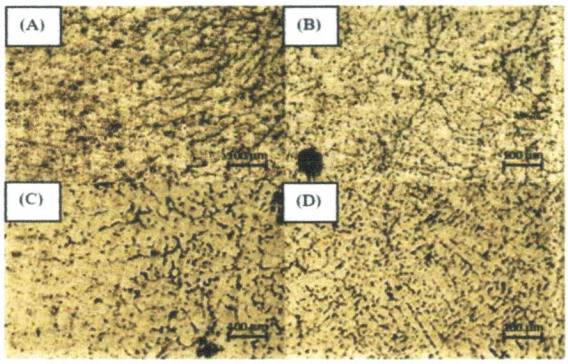

Figure 6 Microstructures of the TIG welded joints before and after repair welding: (A) HAZ AW, (B) WM AW, (C) HAZ RW, and (D) WM RW.

3.3 Hardness test

The hardness profiles of MIG and TIG weldments before and after repair welding are shown in (Figure 7). It can be observed that the hardness variations through WM, HAZ and BM were literally/closely related to the change in microstructure in those zones. The average harnesses of 59, 58.7, 64.7 and 60.7 HV were measured in the WMs of MIG AW, MIG RW, TIG AW and TIG RW, respectively. The composition of ER 4043 filler is ascribed to those hardness values of WMs. However, the WM hardness values of the TIG welded joints were slightly higher than those of the MIG welded joints. The presence of non-equiaxed dendrite grains in the WM of the joints fabricated by the TIG welding as shown in (Figure 6A, 6D) is responsible for higher hardness values. As can be seen in (Figure 7), the PMZs gave the higher hardness than the WMs in all joints. It is directly associated with the availability of Si from the filler to form Mg_2Si precipitates in that zone during recrystallization, which can be seen as deformed grains near the fusion line [21,33]. The lowest hardness was observed in the over-ageing zones of the welded joints where precipitation coarsening or/and phase transformation of $\beta'' \rightarrow \beta' \rightarrow \beta$ in the temperature range 500-240°C was occurred [34,35]. Therefore, it is evident that the over-ageing zones were represented as the weakest regions over the different areas in all joints. As usual, the BM provided the highest hardness over the different regions in all joints due to the supply of hardening precipitates of AA 6082-T6 as discussed previously. The full recovery of the hardness of BM was achieved approximately at 10 mm from the weld center.

It can be seen from the graph that the TIG welded joints produced the lower hardness values in the over-ageing zones than the MIG welded joints. The HAZ hardness of welded joints varied on the difference in microstructures and heat input (welding technique). The higher heat input generated in TIG welding made the cooling rate slower and grain spacing wider in PMZ, resulting in the lower hardness in that zone of the TIG welded joints. In addition, the coarsening of strengthening precipitates observable in the over-ageing zone of the TIG welded joints as shown in (Figure 6A, 6C) exhibited the lower hardness in that zone.

On the other hand, the overall hardness of RW was lower than the AW, especially in the over-ageing zone. The welding thermal cycles subjected were double in the RWs so that it could be expected the more over-ageing effect in that zone of the RW. Moreover, the grain coarsening was observed in the HAZs after repair welding as discussed previous section. Here, it should be noted that the over-ageing zone of MIG welded joints lied at a distance of 8 mm whereas those of TIG welded joints at 7 mm. It is obvious that HAZs of MIG welded joints were slightly wider than those of TIG ones. This phenomenon could be related to different current input modes used in MIG and TIG welding. TIG welding utilizes alternating current polarity during welding whereas MIG welding utilizes direct current. Therefore, the stable heat input generated during MIG welding made the HAZs slightly wider.

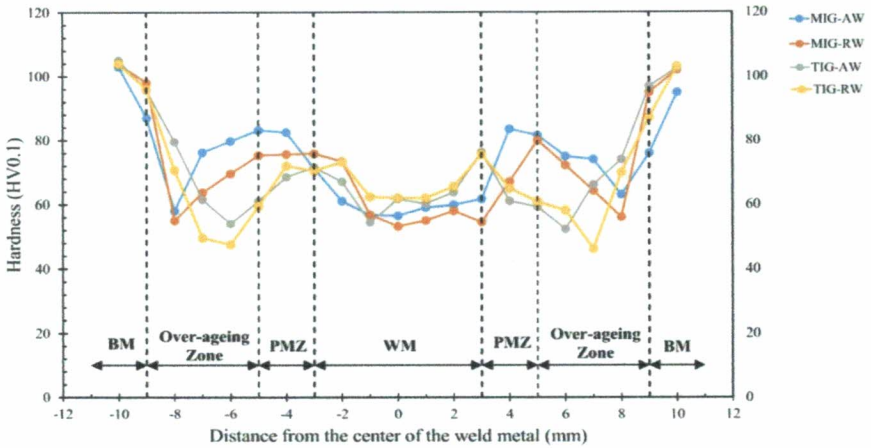

Figure 7 Hardness profiles of the MIG and TIG welded joints of the AA 6082-T6 plates before and after repair welding.

3.4 Tensile properties

The tensile properties of MIG and TIG AWs and RWs are shown in (Table 2). All welded joints fractured at HAZs under tension load as shown in (Figure 8). This is primarily due to the loss of strength in the HAZ by the over-ageing effect during welding. It can be observed that the tensile strength and yield strength of MIG as-weld are 199.6 MPa and 152.5 MPa, respectively, and after repair welding, tensile strength and yield strength decreased to 178. 9 MPa and 145 MPa, respectively. Likewise, a reduction of tensile strength and yield strength were also occurred in TIG welded joints after repair welding. Therefore, it can be inferred that the decrease in strength of welded joints after repair welding must be due to a decrease of hardness in the over-ageing zone resulted from the loss of strengthening constituents, caused by double heat cycles.

Then, the tensile strength and yield strength of TIG welded joints were lower than those of MIG welded joints. These results are consistent with the hardness test. This phenomenon is closely related to lower hardness values in HAZs due to higher heat input generated during welding as discussed above. Moreover, the lower tensile strength is associated with the poor weld reinforcement of the welded joints generated by TIG welding as presented in (Figure 4). Therefore, according to these experimental results, in each welding parameters, the MIG welding is preferred for repairing AA 6082-T6 plates using ER 4043 filler.

Table 2 Tensile properties of the MIG and TIG welded joints of the AA 6082-T6 plates before and after repair welding.

Description	UTS (MPa)	YS (MPa)	% Elongation	Joint Efficiency (%)
AA 6082-T6	310.0	260.0	6.0	-
MIG AW	199.6	152.5	6.6	64.4
MIG RW	178.9	145.0	7.1	57.7
TIG AW	172.2	152.5	7.7	55.5
TIG RW	168.1	141.0	7.7	54.2

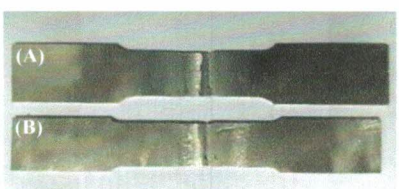

Figure 8 Fracture specimens of (A) MIG RW and (B) TIG RW of the AA 6082-T6.

4. Conclusion

A comparative study on the microstructural characteristics and mechanical properties of 6082-T6 aluminum alloy repair welds fabricated by MIG and TIG welding processes were performed. From the experimental results, the following conclusions can be drawn:

The tensile strength and yield strength of TIG welded joints were lower than those of MIG welded joints. The lower hardness in the HAZs and the poor weld reinforcement of the welded joints generated by TIG welding made the strength of TIG welded joints lower.

A reduction in mechanical strength of AA 6082-T6 welded joints was occurred after repairing regardless of the welding techniques because the hardness of HAZ was decreased after repair welding due to the double welding thermal cycles subjected to RWs.

The hardness of TIG welded joints were lower in the HAZs than MIG welded joints. The microstructurally observable coarsening of strengthening precipitates in the over-ageing zone and the wider grains in PMZ of the TIG welded joints due to the high TIG heat input resulted in the lower hardness in the HAZs of the TIG welded joints.

The HAZ hardness of the repair joints were lower than the as-weld joints irrespective of welding techniques. The grain coarsening in the PMZs and the double over-ageing effect in the over-ageing zones after repair welding were responsible for lowering the hardness.

5. Acknowledgements

Researchers would like to thank Prince of Songkla University for supporting the budget of this research and Department of Mining and Material Engineering, Faculty of Engineering, Prince of Songkla University and Production Technology Program, Faculty of Agriculture and Industrial Technology, Phetchabun Rajabhat University for supporting materials and equipment in the research operation.

6. References

[1] Troeger LP, Starke EA. Microstructural and mechanical characterization of a superplastic 6xxx aluminum alloy. Mater Sci Eng. 2000;277(1):102-113.

[2] Mathers G. The welding of aluminium and its alloys. 1st ed. Oxford: Woodhead Publishing; 2002.

[3] Kaufman JG. Introduction to aluminum alloys and tempers. 1st ed. Almere: ASM International; 2000.

[4] Totten GE, MacKenzie DS. Handbook of aluminum: vol. 1: physical metallurgy and processes. CRC Press. 2003;13-18.

[5] Leoni F, Sandness L, Grong O, Berto F. Mechanical behavior of gas metal arc AA6082-T6 weldments. Procedia Struct Integr. 2019;18(1):449-456.

[6] Huang L, Hua X, Wu D, Jiang Z, Li F, Wang H, et al. Microstructural characterization of 5083 aluminum alloy thick plates welded with GMAW and twin wire GMAW processes. Int J Adv Manuf Technol. 2017; 93(5):1809-1817.

[7] Ambriz RR, Jaramillo D. Mechanical behavior of precipitation hardened aluminum alloys welds. In: Waldemar AM, editor. Light Met Alloys Appl. 1st ed. London: Intech Open; 2014. p. 35-59.

[8] Yürük A, Ayan Y, Çevik B, Kahraman N. Investigation of mechanical and microstructural properties of AA5754/AA6013 dissimilar aluminium alloys joined by GMAW and FSW methods. Kov Mater. 2021;59(4):245-256.

[9] Koprivica A, Bajić D, Šibalić N, Vukčević M. Analysis of welding of aluminium alloy AA6082-T6 by TIG, MIG and FSW processes from technological and economic aspect. Mach Technol Mater. 2020;14(5):194-198.

[10] Heidarzadeh A, Mironov S, Kaibyshev R, Çam G, Simar A, Gerlich AP, et al. Friction stir welding/processing of metals and alloys: a comprehensive review on microstructural evolution. Prog Mater Sci. 2021;117:100752.

[11] Bokov DO, Jawad MA, Suksatan W, Abdullah ME, Świerczyńska A, Fydrych D, et al. Effect of pin shape on thermal history of aluminum-steel friction stir welded joint: computational fluid dynamic modeling and validation. Mater. 2021;14(24):24.

[12] Silva CLM, Scotti A. The influence of double pulse on porosity formation in aluminum GMAWJ Mater Process Technol. 2006;171(3):366-372.

[13] Johnson MS, Santa JF, Mejia OL, Aristizábal S, Ospina S, Cortes PA, et al. Effect of the number of welding repairs with GTAW on the mechanical behavior of AA7020 aluminum alloy welded joints. MMet Mater Trans B. 2015;46(5):2332-2339.

[14] Zhang D, Wu A, Zhao Y, Shan J, Wan Z, Wang G, et al. Microstructural evolution and its effect on mechanical properties in different regions of 2219-C10S aluminum alloy TIG-welded joint. Trans Nonferrous Met Soc China. 2020;30(10):2625-2638.
[15] Chen DL, Chaturvedi MC. Effects of welding and weld heat-affected zone simulation on the microstructure and mechanical behavior of a 2195 aluminum-lithium alloy. Metal Mater Trans A. 2001;32(11):2729-2741.
[16] Shankar K, Wu W. Effect of welding and weld repair on crack propagation behaviour in aluminium alloy 5083 plates. Mater Des. 2002;23(2):201-208.
[17] Katsas S, Nikolaou J, Papadimitriou G. Microstructural changes accompanying repair welding in 5xxx aluminium alloys and their effect on the mechanical properties. Mater Des. 2006;27(10):968-975.
[18] Liu H, Zhang H. Repair welding process of friction stir welding groove defect. Trans Nonferrous Met Soc China. 2009;19(3):563-567.
[19] Yao JG, He DQ, Lai RL, Li R, Wang HJ. Mechanical properties of repairing welding joints of 6005A-T6 aluminum alloy prepared by FSW and MIG processes. Zhongguo Youse Jinshu Xuebao/Chin J Nonferrous Met. 2015;25(3):589-594.
[20] Rayes Mel, El-Danaf E. The Influence of multi-pass friction stir processing on the microstructural and mechanical properties of aluminum alloy 6082. J Mater Process Technol. 2012;212(5):1157-1168.
[21] Baskutis S, Baskutiene J, Bendikiene R, Ciuplys A. Effect of weld parameters on mechanical properties and tensile behavior of tungsten inert gas welded AW6082-T6 aluminium alloy. J Mech Sci Technol. 2019;33(2):765-772.
[22] Wan Z, Meng D, Zhao Y, Zang D, Wang Q, Shan J, et al. Improvement on the tensile properties of 2219-T8 aluminum alloy TIG welding joint with weld geometry optimization. J Manuf Process. 2021;67:275-285.
[23] Shanavas S, Raja Dhas JE. Weldability of AA 5052 H32 aluminium alloy by TIG welding and FSW process -a comparative study. IOP Conf Ser Mater Sci Eng. 2017;247:012016.
[24] Pandey C, Chaurasia PK, Giri A, Saini N, Mahapatra MM. A comparative study of residual stress and mechanical properties for FSW and TIG weld on structural steel. Arch Metall Mater. 2018;63(2):1019-1029.
[25] Sirohi S, Taraphdar PK, Dak G, Pandey C, Sharma SK, Goyal A. Study on evaluation of through-thickness residual stresses and microstructure-mechanical property relation for dissimilar welded joint of modified 9Cr-1Mo and SS304H steel. Int J Press Vessel. 2021;194:104557.
[26] Pandey C, Mahapatra MM, Kumar P, Daniel F, Adhithan B. Softening mechanism of P91 steel weldments using heat treatments. Arch Civ Mech Eng. 2019;19(2):297-310.
[27] Pandey C, Mohan Mahapatra M, Kumar P, Thakre JG, Saini N. Role of evolving microstructure on the mechanical behaviour of P92 steel welded joint in as-welded and post weld heat treated state. J Mater Process Technol. 2019;263:241-255.
[28] Naing TH, Muangjunburee P. Metallurgical and mechanical characterization of MIG welded repair joints for 6082-T6 aluminum alloy with ER 4043 and ER 5356. Trans Indian Inst Met. 2022;75:1583-1593.
[29] Mendelson MI. Average grain size in polycrystalline ceramics. J American Ceramic Society. 1969;52(8): 443-446.
[30] An American National Standard. AWS D1.2/D1.2M:2008, structural welding code-aluminum, https://www.coursehero.com/file/43481765/Structural-Welding-Code-Aluminum-AWS-D1-2pdf/ [accessed 19 June 2021].
[31] Kah P, Olabode M, Hiltunen E, Martikainen J. Welding of a 7025 Al-alloy by a pulsed MIG welding process. J Mech Sci Techno. 2013;19(1):96-103.
[32] Pandey C, Giri A, Mahapatra M. On the prediction of effect of direction of welding on bead geometry and residual deformation of double-sided fillet welds. IJOSS. 2016;16:333-345.
[33] Baskutis S, Zunda A, Kreivaitis R. Mechanical properties and microstructure of aluminium alloy AW6082-T6 joints welded by double-sided MIG process before and after aging. J Mech Sci Technol. 2019; 25(2):107-113.
[34] Missori S, Pezzuti E. Microstructural and mechanical characteristics of welded joints in type 6082-T6 aluminium alloy. Weld Int. 1997;11(6):468-474.
[35] Missori S, Sili A. Mechanical behaviour of 6082-T6 aluminium alloy welds. Metall Sci and Technol. 2000;18(1):12-18.